Comparative Study of Non-linear Controllers Applied to a Six-Phase Induction Machine

Magno Ayala[1], Osvaldo Gonzalez[1], Jorge Rodas[1], Raul Gregor[1], Yassine Kali[2] and Pat Wheeler[3]
[1]Laboratory of Power and Control Systems, Facultad de Ingeniería, Universidad Nacional de Asunción, Paraguay
mayala@ing.una.py, ogonzalez@ing.una.py, jrodas@ing.una.py, rgregor@ing.una.py
[2]École de Technologie Supérieure, Quebec University, Montreal, Canada, y.kali88@gmail.com
[3]Power Electronics, Machines and Control (PEMC) Group, University of Nottinham, UK, Pat.Wheeler@nottingham.ac.uk

***Abstract*—This paper presents a comparative study of two discrete nonlinear current controllers with fixed switching frequency, one based on the model predictive control and the other to robust discrete-time sliding mode, applied to a six-phase induction machine. The outer speed control is based on the proportional-integral controller. Simulation results are presented to demonstrate the performance of the two current control strategies using the mean squared error, root mean square and total harmonic distortion as figures of merit, thus concluding the advantages and limitations of each current controller at steady and transient states.**

***Index Terms*—Discrete time sliding mode, finite state model predictive control, fixed switching frequency, multiphase induction machine, pulse width modulation, space vector modulation.**

NOMENCLATURE

DTSM	Discrete time sliding mode.
FCS-MPC	Finite control set model predictive control.
IGBT	Isolated gate bipolar transistor.
IRFOC	Indirect rotor field oriented control.
KF	Kalman filter.
M2PC	Modulated model predictive control.
MPC	Model predictive control.
MSE	Mean squared error.
PCC	Predictive current control.
PI	Proportional integral.
PWM	Pulse width modulation.
RMS	Root mean square.
SIM	Six-phase induction machine.
SMC	Sliding mode control.
SVM	Space vector modulation.
TDE	Time delay estimation.
THD	Total harmonic distortion.
VSD	Vector space decomposition.
VSI	Voltage source inverter.

I. INTRODUCTION

Multiphase machines have received great interest from power electronics community due to their good features in comparison with traditional three-phase machines such as lower torque ripple, lower current per phase and fault tolerant capabilities [1]–[3]. Nowadays, they are extensively used for high-power and reliable applications such as wind energy conversion systems and electric vehicles [3], [4]. Most of the control strategies applied for multiphase drives in real applications are an extension of the three-phase case such as field oriented control based on proportional-integral current control, direct torque control, among others [5], [6].

In the last few years, some new nonlinear techniques were developed to apply to multiphase machines such as FCS-MPC [7], [8], predictive torque control [9], [10], fuzzy logic control [11] and SMC [11], [12]. Some of these techniques have variants already presented in the literature such as M2PC for FCS-MPC [13] and DTSM for SMC [14] which are considered improved versions on their original techniques. M2PC is based on a modulation scheme, based on SVM, incorporated to the conventional MPC for different power converters [15], [16]. This technique is applied to a two-level VSI, where the duty cycles are generated for two active vectors and two zero vectors which are selected for the converter using a given switching pattern in order to obtain an efficient performance for the SIM [17]. In the case of SMC, it is considered one of the robust proposed nonlinear control techniques in the literature. This technique forces the system trajectories to converge to a user-chosen switching surface [18] in finite-time using a discontinuous controller. However, to ensure high performances, the switching gains should be chosen as large as possible to reject the effect of bounded uncertainties. Therefore, this choice causes the major drawback of SMC, the well-known chattering phenomenon [19].

Recently, a promising idea that consists on combining sliding mode control with TDE method for uncertain nonlinear systems has been presented on [20]. The main contribution of this paper is a comparative study of M2PC, with a KF as an state observer and DTSM, with TDE as an state observer to operate a SIM in terms of current tracking, THD of stator currents and RMS of the current and torque ripple. The two fixed switching frequency techniques are compared by using the MSE, THD and RMS of the current and torque ripple, as figures of merit. These techniques are tested for different operation conditions, in steady state and transient conditions.

This paper is organized as follows: the SIM state-space mathematical model is presented in Section II. In Section III, the M2PC and DTSM designs are shown where, for M2PC it describes the traditional PCC and the modulation method, as for DTSM it explains the technique with TDE. The simulation results are shown in Section IV where the transient and steady

978-1-5386-4191-0/18/$31.00 ©2018 IEEE

state behavior, for the two methods are compared. Section V summarizes the conclusion.

II. Mathematical Model of SIM

The studied system is composed of a SIM connected to a six-leg VSI and a DC voltage source (V_{dc}). An electrical scheme of the VSI drive, based on IGBT, is shown in Fig. 1. The SIM is a continuous system which can be analyzed by differential equations. By considering the VSD technique and the six-dimensional space of the SIM, defined by the six-phases (a, b, c, d, e, f), it can be transformed into three two-dimensional orthogonal planes in the stationary reference frame, represented as ($\alpha-\beta$), ($x-y$) and (z_1-z_2), by using the transformation matrix $\mathbf{T}$ [8]. The studied SIM is asymmetrical and has isolated neutrals configuration, thus (z_1-z_2) currents are not considered.

$$\mathbf{T}=\frac{1}{3}\begin{array}{c}\begin{matrix}a & d & b & e & c & f\end{matrix}\\ \begin{bmatrix} 1 & \frac{\sqrt{3}}{2} & -\frac{1}{2} & -\frac{\sqrt{3}}{2} & -\frac{1}{2} & 0 \\ 0 & \frac{1}{2} & \frac{\sqrt{3}}{2} & \frac{1}{2} & -\frac{\sqrt{3}}{2} & -1 \\ 1 & -\frac{\sqrt{3}}{2} & -\frac{1}{2} & \frac{\sqrt{3}}{2} & -\frac{1}{2} & 0 \\ 0 & \frac{1}{2} & -\frac{\sqrt{3}}{2} & \frac{1}{2} & \frac{\sqrt{3}}{2} & -1 \\ 1 & 0 & 1 & 0 & 1 & 0 \\ 0 & 1 & 0 & 1 & 0 & 1 \end{bmatrix}\end{array}\begin{array}{c}\alpha\\ \beta\\ x\\ y\\ z_1\\ z_2\end{array} \quad (1)$$

where the invariant amplitude criterion has been selected.

The six-phase VSI has a discrete behavior and a total number of $2^6 = 64$ switching states defined by the six VSI legs $\mathbf{S} = [S_a, S_b, S_c, S_d, S_e, S_f]$, where $\mathbf{S}_i \in \{0,1\}$. The different switching states and V_{dc} determine the phase voltages, which can be represented into the ($\alpha-\beta$) and ($x-y$) planes according to the VSD approach [21]. Fig. 2 shows the 64 possibilities which lead only to 49 different vectors (48 vectors + 1 null vector) in the ($\alpha-\beta$) and ($x-y$) planes. The state-space model of the SIM is defined by:

$$\dot{\mathbf{X}}_{(t)} = \mathbf{A}_{(t)}\,\mathbf{X}_{(t)} + \mathbf{B}_{(t)}\,\mathbf{U}_{(t)} + \mathbf{H}\,\varpi_{(t)} \quad (2)$$

where $\mathbf{X}_{(t)} = [x_1, x_2, x_3, x_4, x_5, x_6]^T$ is the state vector that corresponds to the stator and rotor currents $x_1 = i_{\alpha s}$, $x_2 = i_{\beta s}$, $x_3 = i_{xs}$, $x_4 = i_{ys}$, $x_5 = i_{\alpha r}$ and $x_6 = i_{\beta r}$, $\mathbf{U}_{(t)} = [u_1, u_2, u_3, u_4]^T = [v_{\alpha s}, v_{\beta s}, v_{xs}, v_{ys}]^T$ is the input vector applied to the stator, the process noise is defined as $\varpi_{(t)}$ and $\mathbf{H}$ is the noise weight matrix and $\mathbf{A}_{(t)}$ and $\mathbf{B}_{(t)}$ are matrices determined by the electrical parameters of the SIM as follows:

$$\begin{bmatrix} -R_s c_2 & c_4 L_m \omega_r & 0 & 0 & c_4 R_r & c_4 L_r \omega_r \\ c_4 L_m \omega_r & -R_s c_2 & 0 & 0 & c_4 L_r \omega_r & c_4 R_r \\ 0 & 0 & -R_s c_3 & 0 & 0 & 0 \\ 0 & 0 & 0 & -R_s c_3 & 0 & 0 \\ R_s c_4 & -c_5 L_m \omega_r & 0 & 0 & -c_5 R_r & -c_5 L_r \\ -c_5 L_m \omega_r & R_s c_4 & 0 & 0 & -c_5 L_r & -c_5 R_r \end{bmatrix}$$

$$\begin{bmatrix} c_2 & 0 & 0 & 0 \\ 0 & c_2 & 0 & 0 \\ 0 & 0 & c_3 & 0 \\ 0 & 0 & 0 & c_3 \\ -c_4 & 0 & 0 & 0 \\ 0 & -c_4 & 0 & 0 \end{bmatrix}$$

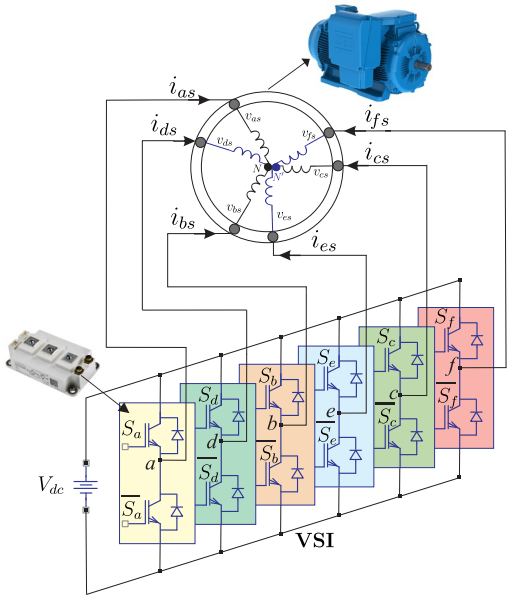

Fig. 1. Scheme of an SIM connected to a six-leg VSI.

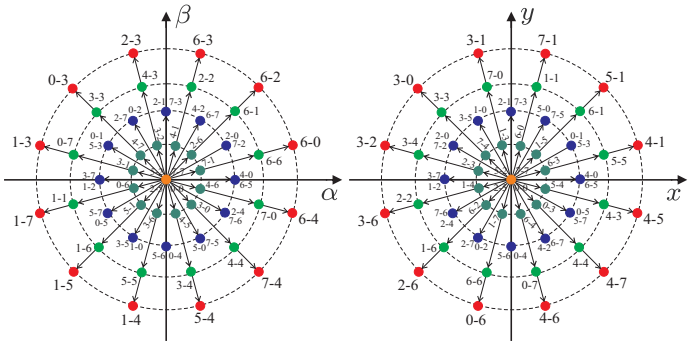

Fig. 2. Voltage space vectors and switching states in ($\alpha-\beta$) and ($x-y$) planes for a SIM.

where R_s, R_r, L_m, $L_r = L_{lr} + L_m$ and $L_s = L_{ls} + L_m$ are the electrical parameters of the SIM. The coefficients are determined as $c_1 = L_s L_r - L_m^2$, $c_2 = \frac{L_r}{c_1}$, $c_3 = \frac{1}{L_{ls}}$, $c_4 = \frac{L_m}{c_1}$ and $c_5 = \frac{L_s}{c_1}$. Stator voltages are dependent of the input control signals $\mathbf{S}$. In this particular case, the simplest VSI model has been considered to obtain a good optimization process. In this model the stator voltages can be calculated from the ideal six-leg VSI model $\mathbf{M}_{[\mathbf{S}]}$ [8].

$$\mathbf{M}_{[\mathbf{S}]} = \frac{1}{3}\begin{bmatrix} 2 & 0 & -1 & 0 & -1 & 0 \\ 0 & 2 & 0 & -1 & 0 & -1 \\ -1 & 0 & 2 & 0 & -1 & 0 \\ 0 & -1 & 0 & 2 & 0 & -1 \\ -1 & 0 & -1 & 0 & 2 & 0 \\ 0 & -1 & 0 & -1 & 0 & 2 \end{bmatrix}\mathbf{S}^T \quad (3)$$

An ideal six-leg VSI transforms gating signals into stator voltages which can be projected to ($\alpha-\beta$) and ($x-y$) planes

and defined in $\mathbf{U}_{(t)}$, determined with the following equation:

$$\mathbf{U}_{(t)} = V_{dc}\,\mathbf{T}\,\mathbf{M}_{[\mathbf{S}]} \tag{4}$$

The output vector, $\mathbf{Y}$, is:

$$\mathbf{Y}_{(t)} = \mathbf{C}\,\mathbf{X}_{(t)} + \nu_{(t)} \tag{5}$$

being $\nu_{(t)}$ is the measurement noise and

$$\mathbf{C} = \begin{bmatrix} 1 & 0 & 0 & 0 & 0 & 0 \\ 0 & 1 & 0 & 0 & 0 & 0 \\ 0 & 0 & 1 & 0 & 0 & 0 \\ 0 & 0 & 0 & 1 & 0 & 0 \end{bmatrix}$$

The mechanical variables of the SIM are related by the following equations:

$$T_e = 3\,P\,(\psi_{\alpha s} i_{\beta s} - \psi_{\beta s} i_{\alpha s}) \tag{6}$$

$$J_i\,\dot{\omega}_m + B_i\,\omega_m = (T_e - T_L) \tag{7}$$

$$\omega_r = P\omega_m \tag{8}$$

where B_i is the friction coefficient, J_i the inertia coefficient, T_e defines the produced torque, T_L is the load torque, ω_r is the rotor electrical speed, ω_m the rotor mechanical speed, $\psi_{\alpha s}$ and $\psi_{\beta s}$ are the stator fluxes and P the number of pole pairs.

III. Proposed Nonlinear Controllers

A. Outer Control Loop

The outer loop is designed for control the speed. A PI controller, designed in [22] is implemented. The PI speed controller is selected to obtain the dynamic reference current $i^*_{qs[k]}$. Then, the process of the slip frequency ($\omega_{sl[k]}$) estimation is executed in the same way as the IRFOC methods, from the reference currents ($i^*_{ds[k]}, i^*_{qs[k]}$) in the dynamic reference frame and the electrical parameters of the SIM.

B. M2PC

1) Classic MPC: This technique uses the mathematical model of the discrete system to predict at time $[k]$ the future values $[k+1]$, by using the measured variables such as stator currents and the mechanical rotor speed.

$$\hat{\mathbf{X}}_{[k+1|k]} = \mathbf{X}_{[k]} + T_s\,f\left(\mathbf{X}_{[k]},\,\mathbf{U}_{[k]},\,\omega_{r[k]}\right) \tag{9}$$

where T_s is the sample time. In the state-space model (9), only the stator currents, voltages and mechanical speed are measured. The stator voltages are predicted from the switching commands issued to the VSI, however, the rotor currents cannot be directly measured. This fact can be solved through a reduced order observer where it provides an estimation for only the rotor currents. This method was proposed in [7] by using a reduced order estimator based on a KF. By considering a zero-mean Gaussian measurement and uncorrelated process noises, the system's equations can be written as:

$$\hat{\mathbf{X}}_{[k+1|k]} = \mathbf{A}_{[k]}\mathbf{X}_{[k]} + \mathbf{B}_{[k]}\mathbf{U}_{[k]} + \mathbf{H}\varpi_{[k]} \tag{10}$$

$$\mathbf{Y}_{[k+1|k]} = \mathbf{C}\,\mathbf{X}_{[k+1]} + \nu_{[k+1]} \tag{11}$$

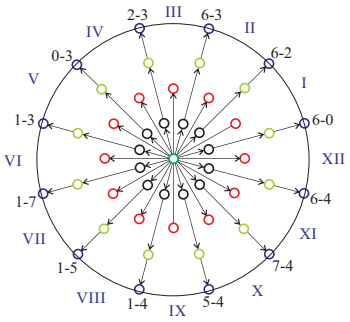

Fig. 3. Available sectors for the six-leg VSI.

where $\mathbf{A}_{[k]}$ and $\mathbf{B}_{[k]}$ are discretized matrices from the model. $\mathbf{A}_{[k]}$ depends on the present value of $\omega_{r[k]}$ and must be considered at every sampling time. A detailed description of the dynamics of the reduced order KF can be found in [7], [23] which has not been presented for the sake of conciseness.

2) Cost Function: The MPC performs an optimization process at every sampling time. This process consists on the evaluation of a cost function (12) for all possible stator voltages to achieve the control objective. The cost function is selected to minimize the current tracking error, defined as the following equation:

$$\begin{aligned} J_{[k+2|k]} =& \parallel i^*_{\alpha s[k+2]} - \hat{i}_{\alpha s[k+2|k]} \parallel^2 + \parallel i^*_{\beta s[k+2]} - \hat{i}_{\beta s[k+2|k]} \parallel^2 \\ &+ \lambda_{xy}\left(\parallel i^*_{xs[k+2]} - \hat{i}_{xs[k+2|k]} \parallel^2 + \parallel i^*_{ys[k+2]} - \hat{i}_{ys[k+2|k]} \parallel^2\right) \end{aligned} \tag{12}$$

being $i^*_{s[k+2]}$ the vector containing the reference for the stator currents and $\hat{i}_{s[k+2]}$ the vector containing the predictions based on the second-step ahead state and a tuning parameter (λ_{xy}) is used [7], [23] to prioritize the $(\alpha - \beta)$ stator currents.

3) Modulation method: It can be determined each available vector for the six-leg VSI in the $(\alpha - \beta)$ plane, which defines 48 sectors, which are given by two adjacent vectors, as shown in Fig. 3. The proposed technique, based on SVM, evaluates the prediction of two active vectors that conform the 12 outside sectors at every sampling time and evaluates the cost function separately. Each prediction is evaluated based on (9) and the only difference is in the calculation of the input vector $\mathbf{U}_{[k]}$ [8].

The duty cycles, for the two active vectors d_1 and d_2, are calculated by solving the next equations:

$$d_0 = \frac{\sigma}{J_0} \qquad d_1 = \frac{\sigma}{J_1} \qquad d_2 = \frac{\sigma}{J_2} \tag{13}$$

$$d_0 + d_1 + d_2 = T_s \tag{14}$$

where d_0 corresponds to the duty cycle of a null vector. Then, it is possible to obtain the expression for σ and the duty cycles for each vector given as:

$$d_0 = \frac{T_s J_1 J_2}{J_0 J_1 + J_1 J_2 + J_0 J_2} \tag{15}$$

$$d_1 = \frac{T_s J_0 J_2}{J_0 J_1 + J_1 J_2 + J_0 J_2} \tag{16}$$

$$d_2 = \frac{T_s J_0 J_1}{J_0 J_1 + J_1 J_2 + J_0 J_2} \tag{17}$$

Considering these expressions, the new cost function, which is evaluated at every T_s, is defined as:

$$G_{[k+2|k]} = d_1 J_1 + d_2 J_2 \tag{18}$$

The two vectors which minimize $G_{[k+2|k]}$ are selected and applied to the six-phase VSI at the next sampling time. After obtaining the duty cycles and selecting the optimal two vectors to be applied, a switching pattern procedure, shown in [24], is adopted with the goal of applying the two active vectors $(v_1 - v_2)$ and two zero vectors (v_0), considering the calculated duty cycles obtaining a fixed-switching frequency.

C. DTSM with TDE

The combination of DTSM control with TDE method will be designed to force the stator current in the $(\alpha-\beta)$ and $(x-y)$ sub-spaces to converge to their desired references in finite-time with high accuracy even in presence of unmeasurable states (rotor currents) and uncertainties. The discrete model of (2) can be expressed as follows:

$$\mathbf{x}_{1[k+1]} = \mathbf{A}_1\, \mathbf{x}_{1[k]} + \mathbf{A}_2\, \mathbf{x}_{3[k]} + \mathbf{B}_1\, \mathbf{v}_{1[k]} + \mathbf{n}_{1[k]} \tag{19}$$

$$\mathbf{x}_{2[k+1]} = \mathbf{A}_3\, \mathbf{x}_{2[k]} + \mathbf{B}_2\, \mathbf{v}_{2[k]} + \mathbf{n}_{2[k]} \tag{20}$$

$$\mathbf{x}_{3[k+1]} = \mathbf{A}_4\, \mathbf{x}_{1[k]} + \mathbf{A}_5\, \mathbf{x}_{3[k]} + \mathbf{B}_3\, \mathbf{v}_{1[k]} + \mathbf{n}_{3[k]} \tag{21}$$

with:

$$\mathbf{x}_{1[k]} = \left[i_{\alpha s[k]},\, i_{\beta s[k]}\right]^T \tag{22}$$

$$\mathbf{x}_{2[k]} = \left[i_{xs[k]},\, i_{ys[k]}\right]^T \tag{23}$$

$$\mathbf{x}_{3[k]} = \left[i_{\alpha r[k]},\, i_{\beta r[k]}\right]^T \tag{24}$$

while the stator voltages represents the input vectors:

$$\mathbf{v}_{1[k]} = \left[v_{\alpha s[k]},\, v_{\beta s[k]}\right]^T \tag{25}$$

$$\mathbf{v}_{2[k]} = \left[v_{xs[k]},\, v_{ys[k]}\right]^T \tag{26}$$

and $\mathbf{H}\, \varpi_{[k]} = \left[\mathbf{n}_{1[k]},\, \mathbf{n}_{2[k]},\, \mathbf{n}_{3[k]}\right]^T \in R^6$. The matrices $\mathbf{A}_1$, $\mathbf{A}_2$, $\mathbf{A}_3$, $\mathbf{A}_4$, $\mathbf{A}_5$, $\mathbf{B}_1$, $\mathbf{B}_2$ and $\mathbf{B}_3$ are discrete forms of sub-matrices from $\mathbf{A}$ and $\mathbf{B}$ defined as follows:

$$\mathbf{A}_1 = \begin{bmatrix} a_{11} & a_{12} \\ a_{21} & a_{22} \end{bmatrix},\ \mathbf{A}_2 = \begin{bmatrix} a_{15} & a_{16} \\ a_{25} & a_{26} \end{bmatrix},\ \mathbf{A}_3 = \begin{bmatrix} a_{33} & 0 \\ 0 & a_{44} \end{bmatrix}$$

$$\mathbf{A}_4 = \begin{bmatrix} a_{51} & a_{52} \\ a_{61} & a_{62} \end{bmatrix},\ \mathbf{A}_5 = \begin{bmatrix} a_{55} & a_{56} \\ a_{65} & a_{66} \end{bmatrix}$$

$$\mathbf{B}_1 = \begin{bmatrix} b_{11} & 0 \\ 0 & b_{22} \end{bmatrix},\ \mathbf{B}_2 = \begin{bmatrix} b_{33} & 0 \\ 0 & b_{44} \end{bmatrix},\ \mathbf{B}_3 = \begin{bmatrix} b_{55} & 0 \\ 0 & b_{66} \end{bmatrix}$$

where:

$a_{11} = a_{22} = 1 - T_s\, c_2\, R_s$ $\quad$ $a_{12} = -a_{21} = T_s\, c_4 L_m\, \omega_{r[k]}$
$a_{15} = a_{26} = T_s\, c_4\, R_r$ $\quad$ $a_{16} = -a_{25} = T_s\, c_4 L_r\, \omega_{r[k]}$
$a_{33} = a_{44} = 1 - T_s\, c_3\, R_s$ $\quad$ $a_{51} = a_{62} = -T_s\, c_4\, R_s$
$a_{52} = -a_{61} = -T_s\, c_5\, L_m\, \omega_{r[k]}$ $\quad$ $a_{55} = a_{66} = 1 - T_s\, c_5\, R_r$
$h_{56} = -h_{65} = -c_5\, \omega_{r[k]}\, T_s\, L_r$ $\quad$ $b_{11} = b_{22} = T_s\, c_2$
$b_{33} = b_{44} = T_s\, c_3$ $\quad$ $b_{55} = b_{66} = -T_s\, c_4$

1) Control of Stator Current in $(\alpha - \beta)$ Sub-Space: To quantify the control objective, let $\mathbf{x}^d_{1[k]} = \left[i^*_{\alpha s[k]},\, i^*_{\beta s[k]}\right]^T$ to be the desired reference and $e_{\phi[k]} = \mathbf{x}_{1[k]} - \mathbf{x}^d_{1[k]} \in R^2$ be the tracking error with $\phi \in \{\alpha, \beta\}$. Then, it is selected the sliding surface [18] to be the error variable as:

$$\sigma_{[k]} = e_{\phi[k]} \tag{27}$$

An ideal sliding motion is ensured if the following conditions is verified:

$$\sigma_{[k]} = 0,\ \sigma_{[k+1]} = 0 \tag{28}$$

where $\sigma_{[k+1]}$ is obtained using the nominal model of (19) as:

$$\begin{aligned} \sigma_{[k+1]} = e_{\phi[k+1]} &= \mathbf{x}_{1[k+1]} - \mathbf{x}^d_{1[k+1]} \\ &= \mathbf{A}_1\, \mathbf{x}_{1[k]} + \mathbf{B}_1\, \mathbf{v}_{1[k]} - \mathbf{x}^d_{1[k+1]} \end{aligned} \tag{29}$$

As the classical sliding motion is not enough to ensure robustness, the following reaching law is chosen:

$$\sigma_{[k+1]} = \lambda\, \sigma_{[k]} - T_s \rho\, \mathrm{sign}(\sigma_{[k]}) \tag{30}$$

where $\lambda = \mathrm{diag}(\lambda_1, \lambda_2)$ with $0 < \lambda_i < 1$ for $i = 1, 2$, $\rho \in R^{2\times 2}$ is a diagonal positive matrix that will be fixed later and $\mathrm{sign}(\sigma_{[k]}) = \left[\mathrm{sign}(\sigma_{1[k]}), \mathrm{sign}(\sigma_{2[k]})\right]^T$ with:

$$\mathrm{sign}(\sigma_{i[k]}) = \begin{cases} 1, & \text{if } \sigma_{i[k]} > 0 \\ 0, & \text{if } \sigma_{i[k]} = 0 \\ -1, & \text{if } \sigma_{i[k]} < 0 \end{cases} \tag{31}$$

Hence, the DTSM controller for the stator current in $(\alpha - \beta)$ sub-space described in (19) is obtained using the nominal model as:

$$\mathbf{v}_{1[k]} = \mathbf{B}_1^{-1} \left[\mathbf{x}^d_{1[k+1]} - \mathbf{A}_1 \mathbf{x}_{1[k]} + \lambda\, \sigma_{[k]} - T_s \rho\, \mathrm{sign}(\sigma_{[k]})\right] \tag{32}$$

Since the rotor currents $\mathbf{x}_{3[k]}$ are not measurable and the vector $\mathbf{n}_{1[k]}$ is unknown, the control performance might not be satisfactory. Then, assuming that $\mathbf{x}_{3[k]}$ and $\mathbf{n}_{1[k]}$ do not vary largely between two consecutive sampling time. Then, using (19), they can be estimated using TDE [25], [26] method as:

$$\begin{aligned} \mathbf{A}_2 \hat{\mathbf{x}}_{3[k]} + \hat{\mathbf{n}}_{1[k]} &\cong \mathbf{A}_2 \mathbf{x}_{3[k-1]} + \mathbf{n}_{1[k-1]} \\ &= \mathbf{x}_{1[k]} - \mathbf{A}_1 \mathbf{x}_{1[k-1]} - \mathbf{B}_1 \mathbf{v}_{1[k-1]} \end{aligned} \tag{33}$$

Definition 3.1: For a discrete system, a quasi sliding mode is considered in the vicinity of the sliding surface, such that $|\sigma_{[k]}| < \varepsilon$, with ε is a positive constant called the quasi-sliding-mode bandwidth. To guarantee a convergent quasi sliding mode, the following sufficient and necessary conditions given in [25], [27] must be verified for $i = 1, 2$:

$$\begin{cases} \sigma_{i[k]} > \varepsilon & \Rightarrow \quad -\varepsilon \le \sigma_{i[k+1]} < \sigma_{i[k]} \\ \sigma_{i[k]} < -\varepsilon & \Rightarrow \quad \sigma_{i[k]} < \sigma_{i[k+1]} \le \varepsilon \\ |\sigma_{i[k]}| \le \varepsilon & \Rightarrow \quad |\sigma_{i[k+1]}| \le \varepsilon \end{cases} \tag{34}$$

Theorem 3.1: The DTSM control with TDE for the stator currents in the $(\alpha - \beta)$ sub-space given in (10) is given by:

$$\begin{aligned} \mathbf{v}_{1[k]} = \mathbf{B}_1^{-1} \big[&\mathbf{x}_{1d[k+1]} - \mathbf{A}_1 \mathbf{x}_{1[k]} - \mathbf{A}_2 \hat{\mathbf{x}}_{3[k]} \\ &- \hat{\mathbf{n}}_{1[k]} + \lambda\, \sigma_{[k]} - T_s \rho\, \mathrm{sign}(\sigma_{[k]})\big] \end{aligned} \tag{35}$$

ensures a quasi sliding mode if the following condition is met:

$$\rho_i > T_s^{-1}\delta_i \quad for\ i = 1, 2 \tag{36}$$

Proof. The proof and the control applied to stator currents in $(x-y)$ sub-space are detailed on [28] thus it has not been presented for the sake of conciseness.

2) PWM Modulation: After DTSM generates the voltage reference in $(\alpha-\beta)$ and $(x-y)$ sub-spaces, it is used a Clark Transformation to obtain the corresponding references per phase. Then it is performed an unipolar voltage PWM to manage the activation of the six-leg VSI.

IV. Simulation Results

A MATLAB/Simulink program has been developed for a SIM in order to compare the proposed methods. A numerical integration using first-order Euler's discretization technique has been applied to compute the evolution of the analyzed system. The parameters of the SIM are: $R_r = 6.9\ \Omega$, $R_s = 6.7\ \Omega$, $L_m = 614$ mH, $P = 1$, $L_{lr} = 12.8$ mH, $L_{ls} = 5.3$ mH, $B_i = 0.0004$ kg.m^2/s, $J_i = 0.07$ kg.m^2, 2 kW of nominal power and 3000 rpm of nominal speed.

In the simulation, V_{dc} is 600 V, the sampling frequency is 16 kHz, a torque load of 2 Nm is connected to the SIM and a d current reference ($i_{ds}^* = 1$ A) has been applied. The PI gains are designed to be $K_P = 0.1050$ and $K_I = 0.1058$. For M2PC, λ_{xy} = 0.01, which is defined in (12), giving more priority to the $(\alpha-\beta)$ stator current tracking. The values of the process noise and the measurement noise can be determined by using the method proposed in [23], being $\hat{Q}_w = 0.0022$ and $\hat{R}_v = 0.0022$. As for DTSM with TDE, these values are considered for stator currents tracking in $(\alpha-\beta)$ sub-space:

$$\lambda = \mathrm{diag}(0.5, 0.5),\ \rho_1 = \rho_2 = 30$$

While the gains of the DTSM for $(x-y)$ currents are:

$$\Gamma = \mathrm{diag}(0.9, 0.9),\ \varrho_1 = \varrho_2 = 30$$

Table I and Table II show a steady state analysis for stator currents, rotor speed and electromagnetic torque under different rotor speed references (ω_r^*) for M2PC and DTSM respectively.

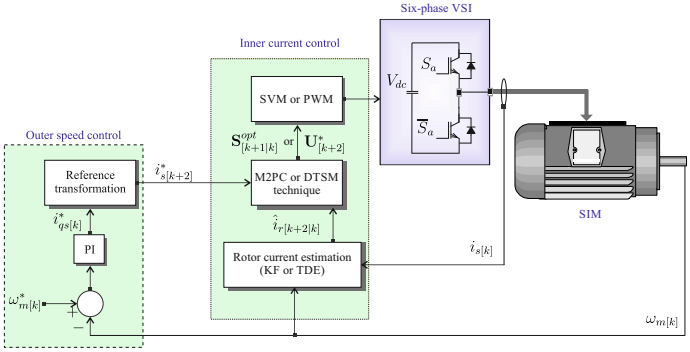

Fig. 4. Speed control with an inner current control based on M2PC or DTSM.

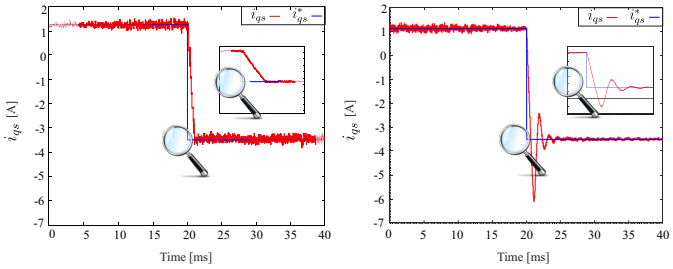

(a) (b)

Fig. 5. Transient response in q-axis stator current for rotor speed of 500 [rpm] to -500 [rpm] and a sampling frequency of 16 [kHz]: (a) M2PC; (b) DTSM.

The results show a good performance at low speed and an average performance at high rotor speed for M2PC, in terms of speed and stator currents tracking (MSE), stator currents THD and torque ripple RMS. As for DTSM, the results denote an better performance, except for speed tracking, at different rotor speeds, compared to M2PC. Fig. 5 exposes the transient response for q stator current in a reversal test (speed reference changes from 500 [rpm] to -500 [rpm]) where M2PC and DTSM have an overshoot of 5 and 71 % and a settling time (5 % criterion) of 10 and 2.9 ms respectively.

TABLE I
Stator Currents $(\alpha-\beta)$, $(x-y)$, MSE [A], THD [%], RMS ripple of T_e [Nm], MSE ω_r [rpm] for M2PC at Different Speeds [rpm].

		Speed ω_r^*	500 [rpm]	
MSE$_\alpha$	MSE$_\beta$	MSE$_x$	MSE$_y$	THD$_\alpha$
0.0949	0.0900	0.3251	0.3651	6.69
THD$_\beta$	MSE$_{\omega_r}$	RMS ripple T_e	RMS ripple T_e %	
6.30	0.1843	0.1001	5.01	
		Speed ω_r^*	1500 [rpm]	
MSE$_\alpha$	MSE$_\beta$	MSE$_x$	MSE$_y$	THD$_\alpha$
0.1869	0.1597	0.4062	0.4485	9.97
THD$_\beta$	MSE$_{\omega_r}$	RMS ripple T_e	RMS ripple T_e %	
9.32	0.8826	0.2042	10.09	

TABLE II
Stator Currents $(\alpha-\beta)$, $(x-y)$, MSE [A], THD [%], RMS ripple of T_e [Nm], MSE ω_r [rpm] for DTSM at Different Speeds [rpm].

		Speed ω_r^*	500 [rpm]	
MSE$_\alpha$	MSE$_\beta$	MSE$_x$	MSE$_y$	THD$_\alpha$
0.0545	0.0547	0.1846	0.1776	5.27
THD$_\beta$	MSE$_{\omega_r}$	RMS ripple T_e	RMS ripple T_e %	
5.31	0.9625	0.0521	2.58	
		Speed ω_r^*	1500 [rpm]	
MSE$_\alpha$	MSE$_\beta$	MSE$_x$	MSE$_y$	THD$_\alpha$
0.0642	0.0651	0.2343	0.2350	5.28
THD$_\beta$	MSE$_{\omega_r}$	RMS ripple T_e	RMS ripple T_e %	
5.41	1.1929	0.0579	2.81	

At last, the behavior of the stator currents in the $(\alpha-\beta)$ and $(x-y)$ sub-spaces are shown in Fig. 6 for M2PC and DTSM

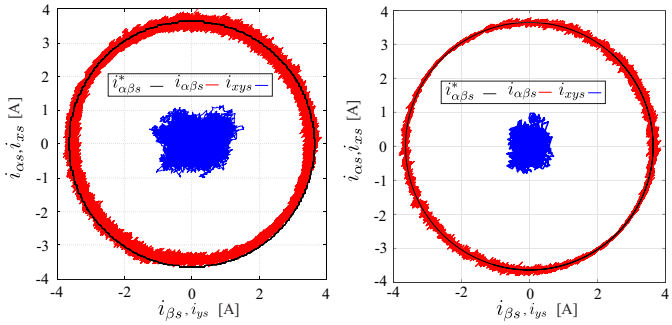

Fig. 6. Stator currents in $(\alpha - \beta)$ and $(x - y)$ sub-spaces for a sampling frequency of 16 kHz with an amplitude of 3.5 A (a) M2PC; (b) DTSM.

in steady-state response. It can be seen a better performance in the $(x - y)$ currents reduction for DTSM.

V. Conclusion

A comparative study of two nonlinear current controllers with fixed switching frequency applied to a SIM is presented. The results were compared between M2PC and DTSM and showed a better performance in terms of current tracking, current THD and torque ripple for DTSM. At the same time, M2PC presented a better capability at lower speed than higher speed. In terms of speed tracking (MSE), M2PC had a slightly better performance than DTSM and in the current transient analysis, M2PC presented a better response than DTSM. It can be stated that both techniques are good options to classic controllers with their corresponding characteristics.

Acknowledgment

Financial support came from CONACYT (Paraguayan Government) through research project 14-INV-101.

References

[1] F. Barrero and M. J. Duran, "Recent advances in the design, modeling, and control of multiphase machines: Part I," *IEEE Trans. Ind. Electron.*, vol. 63, no. 1, pp. 449–458, 2016.

[2] M. J. Duran and F. Barrero, "Recent advances in the design, modeling, and control of multiphase machines: Part II," *IEEE Trans. Ind. Electron.*, vol. 63, no. 1, pp. 459–468, 2016.

[3] E. Levi, "Advances in converter control and innovative exploitation of additional degrees of freedom for multiphase machines," *IEEE Trans. Ind. Electron.*, vol. 63, no. 1, pp. 433–448, 2016.

[4] I. Subotic, N. Bodo, E. Levi, B. Dumnic, D. Milicevic, and V. Katic, "Overview of fast on-board integrated battery chargers for electric vehicles based on multiphase machines and power electronics," *Electric Power Applications*, vol. 10, no. 3, pp. 217–229, 2016.

[5] E. Levi, R. Bojoi, F. Profumo, H. Toliyat, and S. Williamson, "Multiphase induction motor drives–a technology status review," *Electric Power Applications*, vol. 1, no. 4, pp. 489–516, 2007.

[6] A. G. Yepes, A. Vidal, J. Malvar, O. López, and J. Doval-Gandoy, "Tuning method aimed at optimized settling time and overshoot for synchronous proportional-integral current control in electric machines," *IEEE Trans. Power Electronics*, vol. 29, no. 6, pp. 3041–3054, 2014.

[7] J. Rodas, F. Barrero, M. R. Arahal, C. Martín, and R. Gregor, "Online estimation of rotor variables in predictive current controllers: a case study using five-phase induction machines," *IEEE Trans. Ind. Electron.*, vol. 63, no. 9, pp. 5348–5356, 2016.

[8] M. Ayala, J. Rodas, R. Gregor, J. Doval-Gandoy, O. Gonzalez, M. Saad, and M. Rivera, "Comparative study of predictive control strategies at fixed switching frequency for an asymmetrical six-phase induction motor drive," in *Proc. IEMDC*, Miami, FL, 2017, pp. 1–8.

[9] J. A. Riveros, F. Barrero, E. Levi, M. J. Duran, S. Toral, and M. Jones, "Variable-speed five-phase induction motor drive based on predictive torque control," *IEEE Trans. Ind. Electron.*, vol. 60, no. 8, pp. 2957–2968, 2013.

[10] J. Riveros, B. Bogado, J. Prieto, F. Barrero, S. Toral, and M. Jones, "Multiphase machines in propulsion drives of electric vehicles," in *Proc. EPE/PEMC*. IEEE, 2010, pp. T5–201.

[11] M. A. Fnaiech, F. Betin, G.-A. Capolino, and F. Fnaiech, "Fuzzy logic and sliding-mode controls applied to six-phase induction machine with open phases," *IEEE Trans. Ind. Electron.*, vol. 57, no. 1, pp. 354–364, 2010.

[12] H. Amimeur, D. Aouzellag, R. Abdessemed, and K. Ghedamsi, "Sliding mode control of a dual-stator induction generator for wind energy conversion systems," *International Journal of Electrical Power & Energy Systems*, vol. 42, no. 1, pp. 60–70, 2012.

[13] S. Toledo, M. Rivera, J. Muñoz, R. Peña, J. Riveros, and R. Gregor, "Fixed switching frequency predictive control for a multi-drive indirect matrix converter system," in *Proc. SPEC*, pp. 1–6, 2017.

[14] Y. Kali, J. Rodas, M. Saad, R. Gregor, K. Bejelloun, and J. Doval-Gandoy, "Current control based on super-twisting algorithm with time delay estimation for a five-phase induction motor drive,," in *Proc. IEMDC*, 2017, pp. 1–8.

[15] F. Gavilan, D. Caballero, S. Toledo, E. Maqueda, R. Gregor, J. Rodas, M. Rivera, and I. Araujo-Vargas, "Predictive power control strategy for a grid-connected 2L-VSI with fixed switching frequency," in *Proc. ROPEC*, pp. 1–6, 2016.

[16] L. Comparatore, R. Gregor, J. Rodas, J. Pacher, A. Renault, and M. Rivera, "Model based predictive current control for a three-phase cascade H-bridge multilevel STATCOM operating at fixed switching frequency," in *Proc. PEDG*, pp. 1–6, 2017.

[17] M. Rivera, S. Toledo, C. Baier, L. Tarisciotti, P. Wheeler, and S. Verne, "Indirect predictive control techniques for a matrix converter operating at fixed switching frequency," in *Proc. PRECEDE*, pp. 13–18, 2017.

[18] V. Utkin, J. Guldner, and J. Shi, *Sliding mode control in electromechanical systems*. Taylor-Francis, 1999.

[19] I. Boiko and L. Fridman, "Analysis of chattering in continuous sliding-mode controllers," *IEEE Trans. Autom. Control*, vol. 50, pp. 1442–1446, 2005.

[20] Y. Kali, M. Saad, K. Benjelloun, and M. Benbrahim, *Sliding Mode with Time Delay Control for Robot Manipulators*. Singapore: Springer Singapore, 2017, pp. 135–156.

[21] Y. Zhao and T. Lipo, "Space vector PWM control of dual three-phase induction machine using vector space decomposition," *IEEE Trans. Ind. Electron.*, vol. 31, no. 5, pp. 1100–1109, 1995.

[22] L. Harnefors, S. Saarakkala, and M. Hinkkanen, "Speed control of electrical drives using classical control methods," *IEEE Trans. Ind. Appl.*, vol. 49, no. 2, pp. 889–898, 2013.

[23] J. Rodas, C. Martin, M. R. Arahal, F. Barrero, and R. Gregor, "Influence of covariance-based ALS methods in the performance of predictive controllers with rotor current estimation," *IEEE Trans. Ind. Electron.*, vol. 64, no. 4, pp. 2602–2607, 2017.

[24] O. Gonzalez, M. Ayala, J. Doval-Gandoy, J. Rodas, R. Gregor, and G. Rivas, "Variable-speed control of a six-phase induction machine using predictive-fixed switching frequency current control techniques," in *Proc. PEDG*, 2018.

[25] Y. Kali, M. Saad, K. Benjelloun, and A. Fatemi, "Discrete-time second order sliding mode with time delay control for uncertain robot manipulators," *Robotics and Autonomous Systems*, vol. 94, pp. 53 – 60, 2017.

[26] J. H. Jung, P. H. Chang, and S. H. Kang, "Stability analysis of discrete time delay control for nonlinear systems," in *Proc. ACC*, July 2007, pp. 5995–6002.

[27] S. Qu, X. Xia, and J. Zhang, "Dynamics of discrete-time sliding-mode-control uncertain systems with a disturbance compensator," *IEEE Transactions on Industrial Electronics*, vol. 61, no. 7, pp. 3502–3510, July 2014.

[28] Y. Kali, J. Rodas, M. Ayala, M. Saad, R. Gregor, K. Benjelloun, J. Doval-Gandoy, and G. Goodwin, "Discrete-time sliding mode with time delay estimation of a six-phase induction motor drive," in *Proc. IECON (under review)*, 2018.